A monolithic adjusting mechanism for optical element based on modified 6-PSS parallel mechanism

Kang Guo*, Mingyang Ni, Huanan Chen, Yongxin Sui

Engineering Research Center of Extreme Precision Optics, State Key Laboratory of Applied Optics, Changchun Institute of Optics, Fine Mechanics and Physics, Chinese Academy of Science, Changchun 130033, People's Republic of China

ABSTRACT

Adjusting mechanisms with micrometer stroke, nanometer accuracy, high load capacity and compact structure are needed in the deep ultraviolet lithography objective lens. We propose a monolithic adjusting mechanism based on 6-PSS (prismatic-spherical-spherical) parallel mechanism to advisably meet these requirements. Six prismatic joints of the 6-PSS parallel mechanism are optimized into three, which improves the reliability and reduces the cost of the adjusting mechanism. To realize monolithic configuration, a thinned fillet flexure hinge is proposed to work as the spherical joint of the 6-PSS parallel mechanism. This simplifies the alignment process and improves the mechanical accuracy. Structure analysis including positional relationship and transmission ratio is carried out to provide a basis for determining the primary structural dimension of the adjusting mechanism. Verification test results show that the numerical result of the transmission ratio agrees with the experimental one. The axial stroke of the adjusting mechanism is 74.4 μm, the accuracy is within 40 nm, and the surface figure variation of the optical element during the adjusting process is less than 1.5%, which satisfies the operation requirement of the lithography objective lens and shows a bright prospect to actuate other objects in the applications of micro-nano.

© 2016 Elsevier B.V. All rights reserved.

1. Introduction

Adjusting mechanisms are widely applied in optical system for function alteration or performance amelioration. In deep ultraviolet lithographic objective lens, which is an ultra-precise optical system, continuous accuracy promotion is required for adjusting mechanisms to meet the technological conditions of the ever-smaller feature line width in the great large scale integrated circuit fabrication [1]. Presently, the adjusting stroke of the adjusting mechanism applied in the deep ultraviolet lithographic objective lens is of micrometer level, and the adjusting accuracy is in the range of nanometer [2,3]. Moreover, multiple optical elements in the deep ultraviolet lithographic objective lens are strung in a group along the optical axis. The axial interval of the optical elements is mostly of a few millimeters [4]. Therefore, each mechanical structure for supporting or adjusting the optical element has limited axial space to avoid physical interference with the upper or subjacent optical element. These factors enlarge the difficult for the development of the adjusting mechanism.

Conventional adjusting mechanisms such as lead screw and nut, worm, rack-and-pinion and cam are short of adjusting accuracy and bulk volume. For example, Guo et al. [5] developed a mirror focusing mechanism applied in space camera by using lead screw and nut, the resolution of the focusing mechanism is 0.5 μm. Su et al. [6] designed a cam mechanism for lens in infrared zoom system with the adjusting precision of 5 μm. In order to achieve nanoscale adjusting accuracy, flexible mechanism is generally utilized. Hale et al. [7] developed a three-degree-of-freedom optic mechanism with resolution of less than 10 nm in translation and less than 30 nrad in rotation for extreme ultraviolet lithography applications. The optic of the mechanism is aligned by three identical monolithic flexure mechanisms which assembled at three points around the periphery of the optic cell. Gaunekar et al. [8] proposed a lens focusing mechanism employed in semiconductor wire bonding device. The mechanism is guided by a pair of flexure bearings and actuated by a voice coil motor. The central moving portion and the outer section of the two flexure bearings are assembled to the lens supporting tube and the housing of the focusing mechanism, respectively. Noll et al. [9] presented a mirror positioning stage for synchrotron optics in ultrahigh vacuum with nanometer accuracy. The stage is supported and driven by six struts which constituted a layout combined by parallelogram and trapezoidal arrangement.

Due to the complex structure, the above mentioned mechanisms are hard to be developed for monolithic configuration. Consequently, assembly process should be taken for their production, which introduces error and reduces the mechanical accuracy of the mechanisms. Efforts have been taken by researchers to design monolithic adjusting mechanism for optical element, but they are only realized in miniaturization applications [10–13] or microminiaturization applications [14,15], at present. This paper proposes a monolithic adjusting mechanism for optical elements with diameter of hundred millimeters used in the deep ultraviolet lithographic objective lens to regulate the axial interval of the optical elements and compensate the magnification, astigmatism, distortion and spherical aberration of the lens optical system. The proposed adjusting mechanism is designed based on a modified 6-PSS parallel mechanism. Parallel mechanism is a category of mechanism with its stationary base and end-effector connected by at least two kinematic chains, and its actuations located on at least two kinematic chains [16,17]. Compared with series mechanism which has only one kinematic chain, parallel mechanism owns significant characteristics of compact structure, large load capacity, fast response and high mechanical precision [18–21]. These features make the parallel mechanism advisable for working as the adjusting mechanism in the lithographic objective lens. Structure and working principle of the adjusting mechanism are analyzed, and a prototype of the adjusting mechanism is fabricated for experimental verification.

2. Structure design

2.1. 6-PSS parallel mechanism and its modification

The 6-PSS parallel mechanism is composed of 6 pieces of kinematic chain. Each kinematic chain includes a prismatic joint (P) and two spherical joints (S), as shown in Fig. 1(a). If six prismatic joints synchronously translate forward or backward with same displacement, the end-effector of the parallel mechanism will be able to move upwards or downwards in the axial direction (z). The significant advantage of the 6-PSS parallel mechanism for being worked as an adjusting mechanism is that actuators can be fixed on the stationary base to provide linear displacement for the prismatic

joints, and the optical element can be mounted on the end-effector without aperture occupied by structure.

Generally, 6 pieces of actuators should be employed to drive 6 prismatic joints in the 6-PSS parallel mechanism and gain 6 degree-of-freedom (DOF) motions. However, in adjusting mechanism for optical element, only axial motion of the 6-PSS parallel mechanism is desired. In order to reduce the number of the actuator which improves the reliability of the mechanism and reduces the cost of the adjusting mechanism, the 6-PSS parallel mechanism is modified. 6 pieces of kinematic chain are divided into three groups. Each group shares a prismatic joint, and each prismatic joint is driven by an actuator, as shown in Fig. 1(b). As a result, 6 pieces of actuators in conventional 6-PSS parallel mechanism are decreased into 3 pieces. The shared prismatic joints change the DOF of the adjusting mechanism, but the motion characteristics of the adjusting mechanism in the axial direction are not affected.

The DOF of the modified 6-PSS parallel mechanism can be calculated by Grübler-Kutzbach formula [22].

$$M = 6 \times (n - g - 1) + \sum_{i=1}^{g} f_i \qquad (1)$$

Wherein, M represents the number of the DOF, n is the number of the structural parts, g is the number of the kinematic joints between the structural parts, f_i represents the number of relative DOF of the i-th kinematic joint. For the 6-PSS parallel mechanism shown in Fig. 1(b), $n = 11$ (including an end-effector, 6 rigid linkages, 3 shafts for three prismatic joints and a stationary base), $g = 15$ (including 12 spherical joints and 3 prismatic joints), for spherical joint $f_i = 3$, prismatic joint $f_i = 1$. Substituting these values into Eq. (1), one gets $M = 9$. However, there is a local rotational DOF between the two spherical joints of each kinematic chain, 6 local DOF should be subtracted in the above result. Eventually, the nominal DOF of the adjusting mechanism is 3.

2.2. Design of the adjusting mechanism

The adjusting mechanism for optical element based on 6-PSS parallel mechanism with shared prismatic joint is shown in Fig. 2. The adjusting mechanism is of applanate and monolithic configuration. Three groups of kinematic chain are evenly circumferential
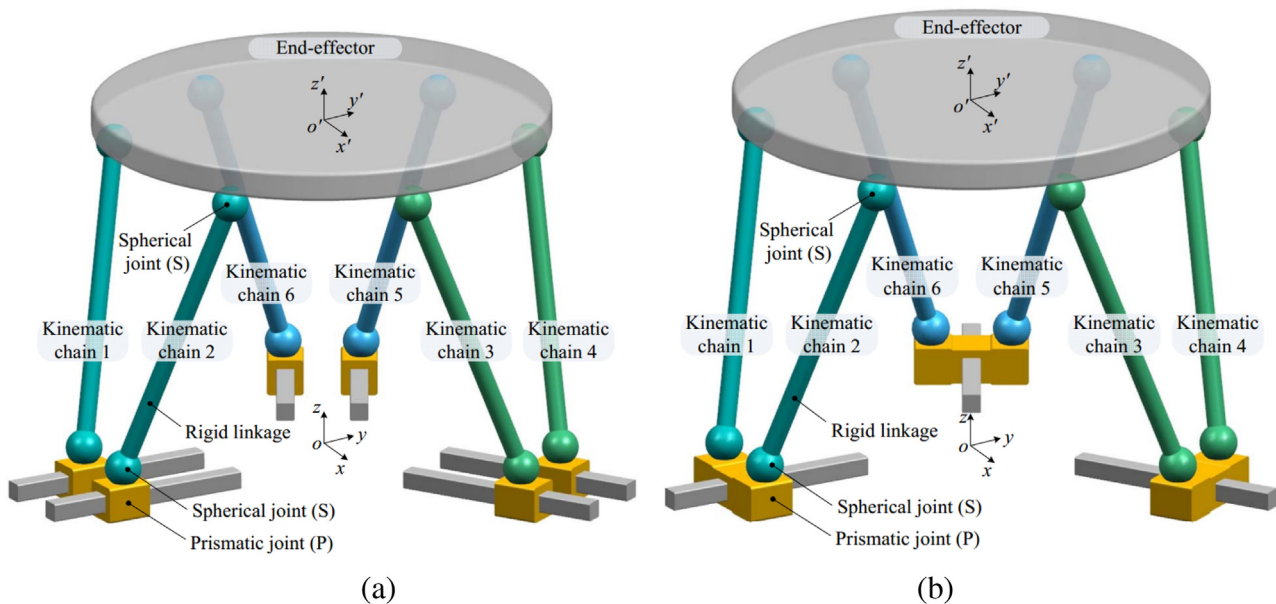

Fig. 1. Diagram of the 6-PSS parallel mechanism: (a) conventional 6-PSS parallel mechanism, (b) modified 6-PSS parallel mechanism with shared prismatic joints.
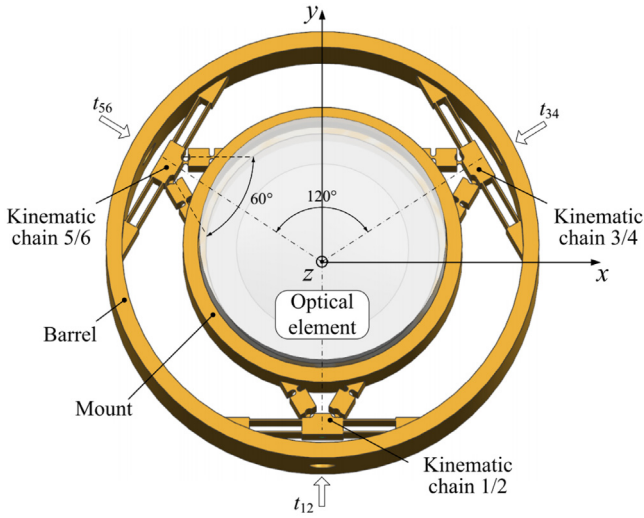
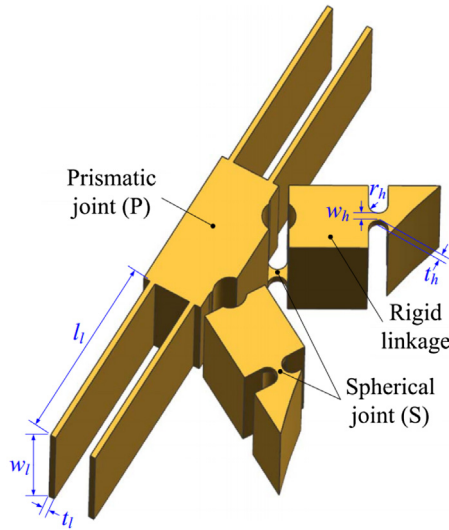**Fig. 2.** Configuration of the adjusting mechanism for the optical element.

Fig. 3. Configuration of the realistic kinematic chain.

Fig. 4. Thinned fillet flexure hinge with three rotational DOF.

Fig. 5. The schematic and geometrical description of the 6-PSS parallel mechanism with shared prismatic joints.

tion for the two spherical joints in each kinematic chain, as shown in Fig. 3, or the axial motion cannot be generated by the 6-PSS parallel mechanism.

3. Analysis of the adjusting mechanism

3.1. Position analysis of the adjusting mechanism

The positional relationship between the input component and the output component is the main factor for the stroke design and the selection of actuator for the adjusting mechanism. It is analyzed based on space vector method in this section. Fig. 5 shows the schematic and geometrical description of the 6-PSS parallel mechanism with shared prismatic joints. Where A_1–A_6 present the spherical joints on the end-effector, B_1–B_6 present the spherical joints connected to the prismatic joints. The coordinate system of the stationary base is o-xyz, and o'-$x'y'z'$ for the coordinate system of the end-effector. r is the radius of the circle generated by A_1–A_6, α is the circumferential included angle of two spherical joints on the end-effector of each group of kinematic chains, w_b is the spacing of two spherical joints connected to a shared prismatic joint, d_b is distance between the origin o and the midpoint of the two spherical joints connected to a shared prismatic joint, l is the linear distance between two spherical joints of each kinematic chain, l_b is the projection distance in the horizontal plane of two spherical joints of each kinematic chain, and b is the projection distance in the axial direction of two spherical joints of each kinematic chain. The following relations exist among the above mentioned geometric parameters.

Supposing the translations of the end-effector along the x, y and z-axis are x_p, y_p and z_p, and the rotations about the x, y and z-axis

The adjusting mechanism has six kinematic chains distributed between the barrel (stationary base) and the mount (end-effector). Two kinematic chains of each group are symmetrical along the radial direction of the optical element with an included angle of 60° to enhance the stability of the mechanism.

The prismatic joint of each kinematic chain is realized by a parallel flexible leaf, as shown in Fig. 3. The parallel flexible leaf provides precise guiding for the actuator and steady supporting for the inner structure. It can be easily electro discharge machined (EDM) along the axial direction. For the realization of spherical joint, a thinned fillet flexure hinge is proposed, as shown in Fig. 4. As is known to all, the fillet flexible hinge has a rotational freedom θ_z around the thickness direction of the hinge. When the fillet flexible hinge is thinned in the thickness direction, two freedoms are newly generated, that is the bending freedom θ_y about the width direction and the torsional freedom θ_x about the length direction. Consequently, the thinned fillet flexure hinge gets three rotational DOF, which makes it possible to be worked as the spherical joint in the 6-PSS parallel mechanism. The thinned fillet flexure hinge can be manufactured by milling, drilling, reaming and electro discharge machining all along the axial direction. This creates the feasibility to achieve monolithic configuration for the adjusting mechanism. It is worth noting that there is altitude difference in the axial direc-
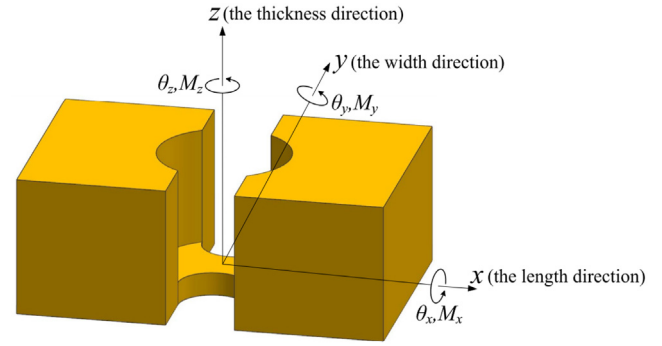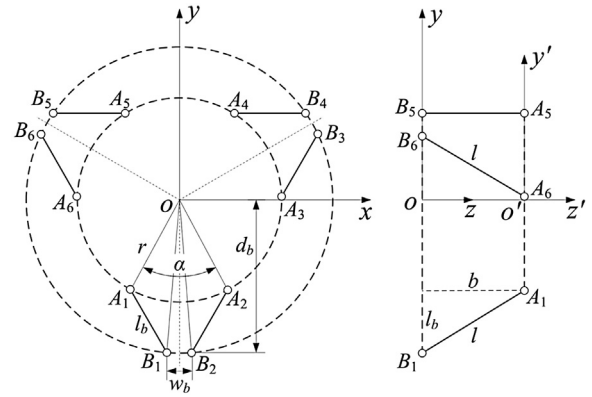
are α, β and γ, the position of the each spherical joint on the end-effector is expressed as:

$$\begin{cases} r\sin\dfrac{\alpha}{2} - \dfrac{w_b}{2} = l_b \sin\dfrac{\pi}{6} \\ d_b - r\cos\dfrac{\alpha}{2} = l_b \cos\dfrac{\pi}{6} \end{cases} \tag{2}$$

$$\begin{bmatrix} x_{Ai} \\ y_{Ai} \\ z_{Ai} \end{bmatrix} = R \begin{bmatrix} x_{Ai}' \\ y_{Ai}' \\ z_{Ai}' \end{bmatrix} + \begin{bmatrix} x_p \\ y_p \\ z_p \end{bmatrix} + \begin{bmatrix} 0 \\ 0 \\ b \end{bmatrix} \quad (i = 1, 2, \ldots, 6) \tag{3}$$

Where $\begin{bmatrix} x_{Ai} & y_{Ai} & z_{Ai} \end{bmatrix}^T$ is the coordinate vector of A_1–A_6 in the coordinate system of the stationary base, $\begin{bmatrix} x_{Ai}' & y_{Ai}' & z_{Ai}' \end{bmatrix}^T$ is the coordinate vector of A_1–A_6 in the coordinate system of the end-effector, $\begin{bmatrix} 0 & 0 & b \end{bmatrix}^T$ is the coordinate vector of the end-effector in the coordinate system of the stationary base, the rotation transformation matrix R between the coordinate system of the end-effector and stationary base is taken as:

$$R = \begin{bmatrix} \cos\alpha\cos\beta & \cos\alpha\sin\beta\sin\gamma - \sin\alpha\cos\gamma & \cos\alpha\sin\beta\cos\gamma + \sin\alpha\sin\gamma \\ \sin\alpha\cos\beta & \sin\alpha\sin\beta\sin\gamma + \cos\alpha\cos\gamma & \sin\alpha\sin\beta\cos\gamma - \cos\alpha\sin\gamma \\ -\sin\beta & \cos\beta\sin\gamma & \cos\beta\cos\gamma \end{bmatrix} \tag{4}$$

$\begin{bmatrix} x_{Ai}' & y_{Ai}' & z_{Ai}' \end{bmatrix}^T$ can be obtained according to the structural dimensions of the adjusting mechanism. Then, $\begin{bmatrix} x_{Ai} & y_{Ai} & z_{Ai} \end{bmatrix}^T$ can be calculated according to Eq. (3).

Supposing the displacement of each prismatic joint is t_{12}, t_{34} and t_{56}, as shown in Fig. 2, $\begin{bmatrix} x_{Bi} & y_{Bi} & z_{Bi} \end{bmatrix}^T$ which presents the coordinate vector of B_1–B_6 in the coordinate system of the stationary base can be given out. During the operation of the 6-PSS parallel mechanism, l which presents the length the rigid linkage is constant. According to the structure vector relationship of the parallel mechanism, a kinematic constraint equation can be established as below.

$$(x_{Ai} - x_{Bi})^2 + (y_{Ai} - y_{Bi})^2 + (z_{Ai} - z_{Bi})^2 = l^2 (i = 1, 2, \ldots, 6) \tag{5}$$

If the posture of the end-effector is known, i.e. x_p, y_p, z_p, α, β and γ is given out, substituting the coordinates of A_1–A_6 and B_1–B_6 with respect to the coordinates of the origin o into Eq. (5), the value of t_{12}, t_{34} and t_{56} can be determined. Accordingly, the positional relationship between the input component and the output component of the adjusting mechanism is obtained.

3.2. Transmission ratio of the adjusting mechanism

In the adjusting mechanism, only the axial motion of the 6-PSS parallel mechanism is utilized. This means the posture parameters x_p, y_p, α, β and γ of the end-effector are specified to be zero. Moreover, as described in Section 2.1, to gain axial motion of the 6-PSS parallel mechanism, the input of the three prismatic joints should be synchronous and equivalent. It indicates that the displacements of each prismatic joint t_{12}, t_{34} and t_{56} are equal to each other, i.e. $t_{12} = t_{34} = t_{56}$. Substituting the posture parameters and the equality into Eq. (5), the displacements of each prismatic joint $t = t_{12} = t_{34} = t_{56}$ can be solved as:

$$t^2 - \sqrt{3} l_b t + z_p^2 + 2b z_p = 0 \tag{6}$$

By solving Eq. (6), one gets:

$$t = \frac{\sqrt{3}}{2} l_b \pm \sqrt{\frac{3}{4} l_b^2 + b^2 - (z_p + b)^2} \tag{7}$$
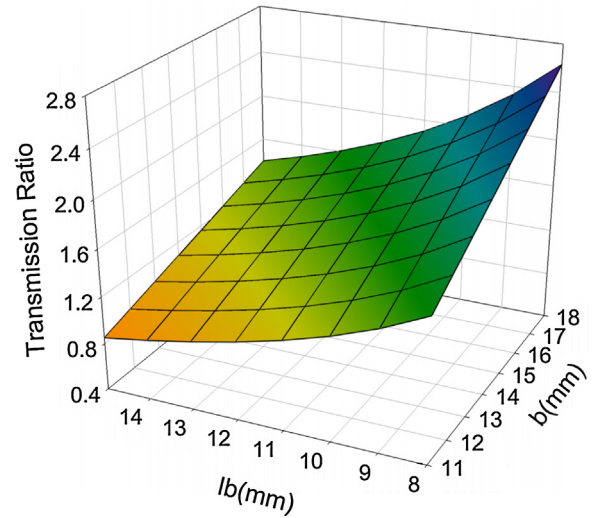

Fig. 6. Relationship between the theoretical transmission ratio and the structural dimensions of the adjusting mechanism.
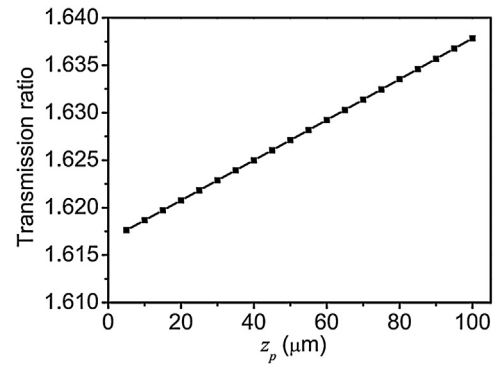

Fig. 7. Relationship between the theoretical transmission ratio and the stroke of the adjusting mechanism.

The $\pm$ sign in Eq. (7) indicate that multiple solutions for the input displacement t_{12}, t_{34} and t_{56} are existed to obtain an output displacement z_p. Actually, the positive sign in Eq. (7) means that $B_1 \sim B_6$ move towards the origin o and cross A_1–A_6 in the radial direction. It is not desirable in practical application. While the negative sign in Eq. (7) means that B_1–B_6 move towards the origin o but always located outside of A_1–A_6 in the radial direction. It meets the actual requirement that the adjusting mechanism does not affect the aperture of the optical element. Therefore, the practically feasible solution of Eq. (6) is as follows:

$$t = \frac{\sqrt{3}}{2} l_b - \sqrt{\frac{3}{4} l_b^2 + b^2 - (z_p + b)^2} \tag{8}$$

It shows in Eq. (8) that the transmission ratio R_a of the adjusting mechanism, which is taken as $R_a = t/z_p$, is only related to l_b and b.

In this research, the adjusting mechanism is designed for actuating an optical element with the outer diameter of 90 mm, and the quality of 0.4 kg. The required adjusting stroke is 60 μm, and the adjusting accuracy is within 50 nm. When $z_p = 60$ μm, the relationship between R_a and l_b, b is shown in Fig. 6.

Considering the adjusting stroke, the selection of the actuator and the match of the structure and the optical element, l_b is determined as 10 mm, and b is taken as 14 mm in this research. According to Eq. (8), when z_p ranges from 0 to 100 μm, the variation trend of the transmission ratio is shown in Fig. 7. With the output displace-
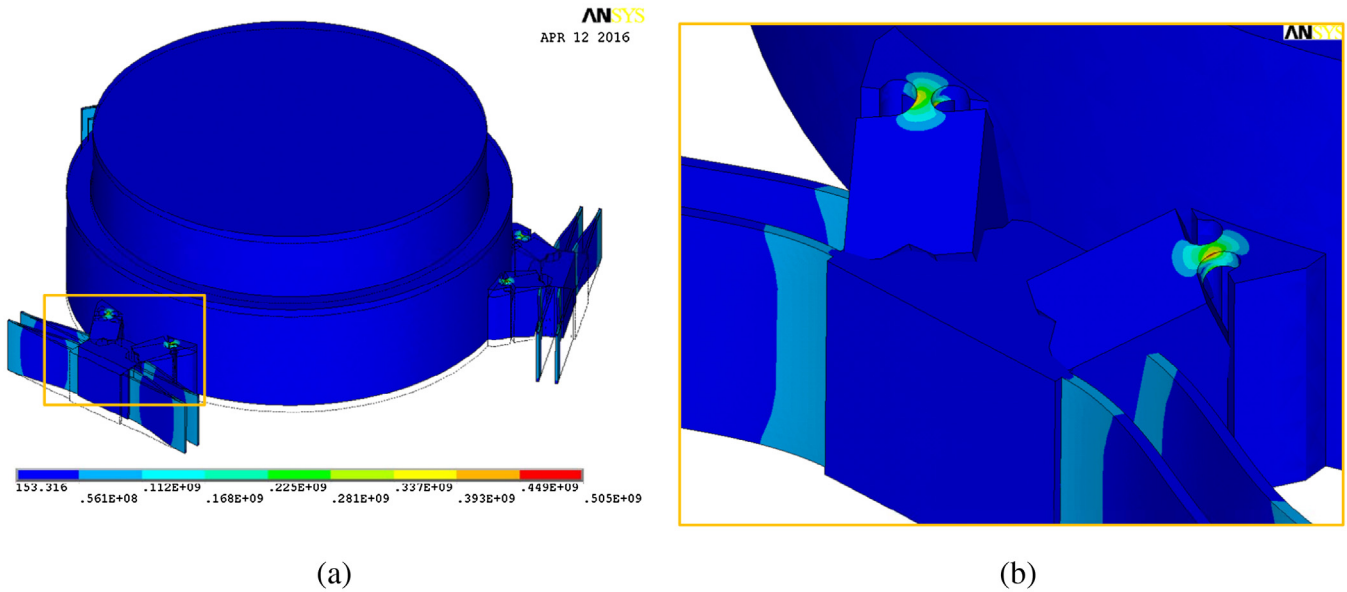
Fig. 8. Axial deformation and stress distribution of the adjusting mechanism: (a) the full view of the adjusting mechanism, (b) the partial enlarged view focusing on the stress distribution of the joints.
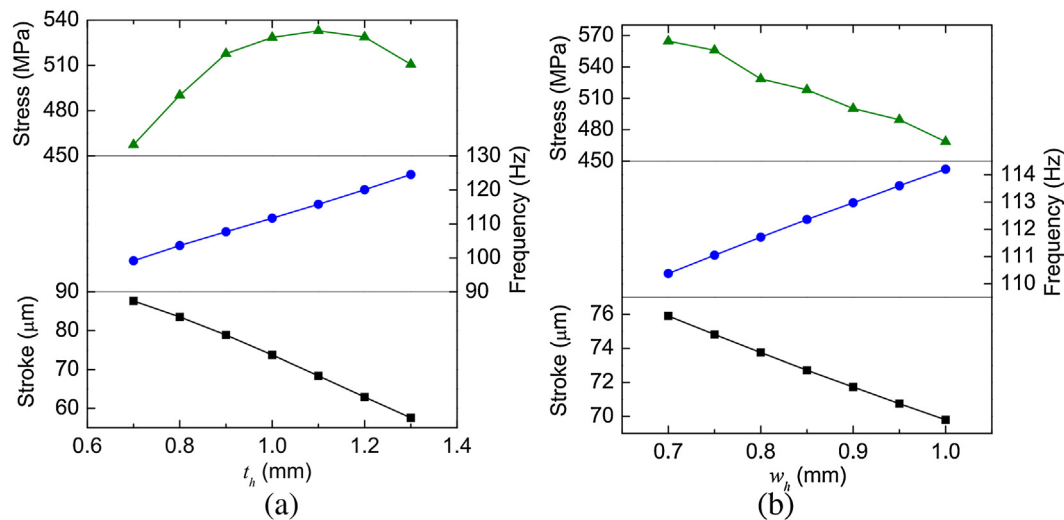

Fig. 9. Relationship between the geometries of the thinned fillet flexure hinge and the characteristics of the adjusting mechanism: (a) thickness, (b) width.

ment increases, the transmission ratio increases linearly, and the variation amplitude is within 1.5%.

3.3. Finite element analysis

The finite element model of the adjusting mechanism is adopted to investigate the relationship between the geometries and the characteristics of the adjusting mechanism, furthermore, determine the structural parameters, especially the flexible joint parameters of the adjusting mechanism. The main geometry parameters are listed in Table 1. The noticeable characteristics of the adjusting mechanism in the lithographic objective lens are the adjusting stroke, the natural frequency and the von Mises stress.

Fig. 8 shows the axial deformation and the stress distribution plot of the adjusting mechanism (without barrel for calculation simplification) analyzed by ANSYS software. Where, the chromatic entity indicates the deformed shape, and the hairlines denote the undeformed edge. It can be seen that, the deformation mainly

Table 1
Main parameters of the adjusting mechanism.

Material parameters (stainless steel)			
Young's modulus	Yield strength	Poisson's ratio	Density
206 GPa	520 MPa	0.29	7.74×10^3 kg/m³

Geometric parameters (mm)					
r		α	w_b	d_b	l_b	b
55		20.7	10	62.8	10	14

occurs at the flexible leaves and the thinned fillet flexure hinges, while the rigid linkages, the mount and the optical element do not have significant deformation. Therefore, we can focus our attention on the flexure joint part of the adjusting mechanism.

The relationships between the geometries of the flexure joint part and the characteristics of the adjusting mechanism are explored by finite element analysis. The geometries of the flexure joint part are presented in Fig. 3. Where, l_l, w_l and t_l present
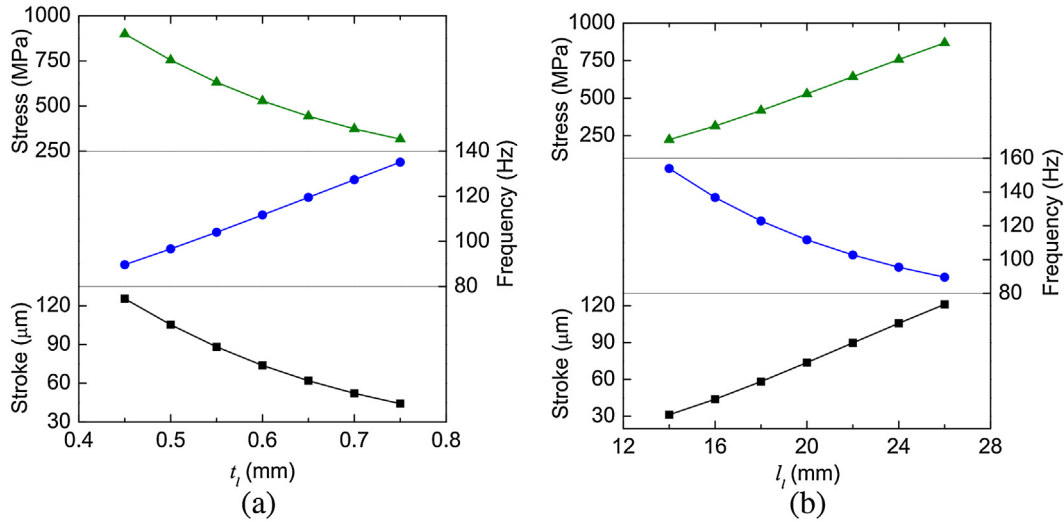
Fig. 10. Relationship between the geometries of the flexible leaf and the characteristics of the adjusting mechanism: (a) thickness, (b) length.

Table 2
Preferred flexible joint parameters of the adjusting mechanism.

Geometric parameters	l_l	w_l	t_l	r_h	w_h	t_h
Value (mm)	20	14	0.6	1	0.8	1

the length, width and thickness of the flexible leaves, respectively. And r_h, w_h and t_h present the cutting radius, width and thickness of the thinned fillet flexure hinges, respectively. The input force applied on each prismatic joint is 50N. r_h is set as 1 mm, and w_l is equal to the altitude difference of the two spherical joints in each kinematic chain, which is 14 mm. The results are shown in Fig. 9 for the thinned fillet flexure hinge, and Fig. 10 for the flexible leaf, respectively. We can see in Figs. 9 and 10 that with the raise of the adjusting stroke, the natural frequency decreases and the von Mises stress increases, except for the relationship between t_h and the von Mises stress. Normally, under a fixed load, with the decrease of t_h, the von Mises stress increases. When t_h decreases and approaches w_h, the stress concentration effect of the fillet flexure hinge is the highest. Then, with the stress concentration effect reduces, the von Mises stress of the thinned fillet flexure hinge decreases.

By evaluating the performance tradeoff among the characteristics of the adjusting mechanism, the geometries of the flexible joints are determined as shown in Table 2. Under these geometries, the stroke of the adjusting mechanism is 73.75 μm, the natural frequency is 111.7 Hz and the von Mises stress is 496.4 MPa.

4. Experiments

4.1. Experimental setup

The prototype of the adjusting mechanism for the optical element is shown in Fig. 11(a) and (b) shows the enlarged image of the thinned fillet flexure hinge captured by image measuring instrument. Three piezoelectric actuators (model N-111.20 with drive force of 50N and travel range of 10 mm, from PI (Physik Instrumente), Inc.) with controller (model E-712, from PI, Inc.) are employed for the displacement input of the prismatic joints. Three single-probe capacitive sensors (model D-E30.500 with a resolution of 4 nm and linearity better than 0.05% over a measuring range of 500 μm, from PI, Inc.) with controller (model E-509, from PI, Inc.) are adopted to detect the axial displacement of the mount. The three capacitive sensors are alternately arranged with the three piezoelectric actuators, so they can also detect the coupled tip and

tilt motion of the mount. Theoretically, there is no tip or tilt motion if the displacement increments detected by each capacitive sensor are equal. Therefore, a PID (proportional-integral-derivative) procedure for closed loop control is prepared to suppress the coupled tip or tilt motion as much as possible in actual application. The experimental setup is shown in Fig. 12.

4.2. Adjusting stroke and accuracy

Appling maximum drive force of 50N on the adjusting mechanism by three piezoelectric actuators, the maximum stroke of the optical element with no tip and tilt error detected by the capacitive sensors is 74.4 μm. That is the adjusting stroke of the adjusting mechanism.

The adjusting accuracy of the adjusting mechanism is mainly affected by the manufacturing precision of the monolithic structure, the driving accuracy of the piezoelectric actuator, the measurement accuracy of the capacitive sensor, and the efficiency of the closed-loop control. Taking the actual tested adjusting accuracy under typical adjusting stroke for example, the measurement curves of each capacitive sensor during the adjusting process are shown in Fig. 13(a) under the adjusting stroke of 10 μm, and Fig. 13(b) under the adjusting stroke of 20 μm. We can see the adjusting process is completed within 200 ms towards the adjusting stroke of 10 μm, and 300 ms towards the adjusting stroke of 20 μm. There is a divergence in the inserted graphs in Fig. 13. It is mainly due to the different noise and drift performance of the different capacitive sensors, originated from the different installation condition and demodulator difference of the capacitive sensors. However, the amplitudes of the noise and drift of the capacitive sensors are all within 0.04 μm (40 nm). Therefore, it indicated that the adjusting accuracy of the adjusting mechanism is able to achieve less than 40 nm.

4.3. Transmission ratio

The actual transmission ratio of the adjusting mechanism is influenced by the dimension error after fabrication. Therefore, there are differences between the transmission ratios for each kinematic chain. To get the actual transmission ratio, each piezoelectric actuator drives the adjusting mechanism independently to obtain the relationship between the individual actuator and the three sensors. Then, the transmission matrix between the input and output
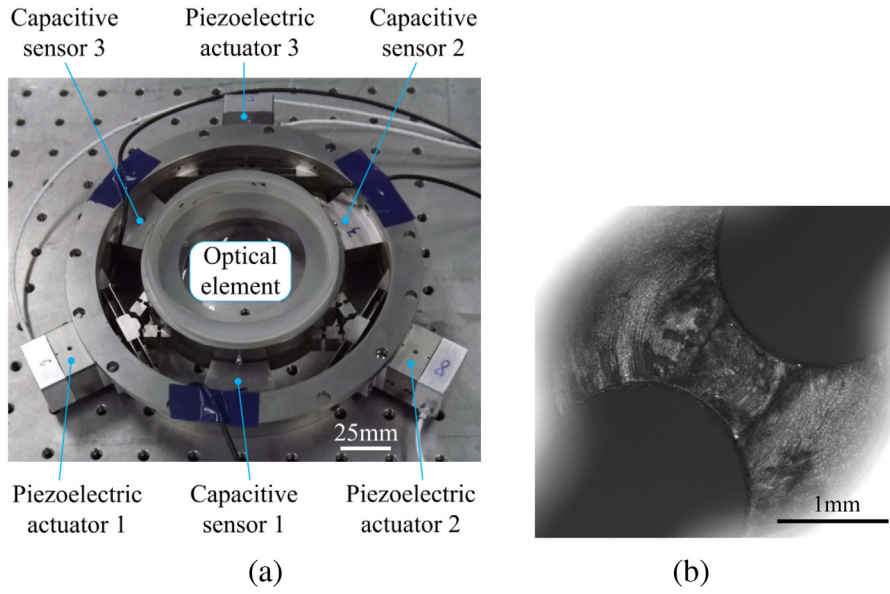
Fig. 11. Prototype of the adjusting mechanism: (a) the full view of the adjusting mechanism, (b) the enlarged image of the thinned fillet flexure hinge.
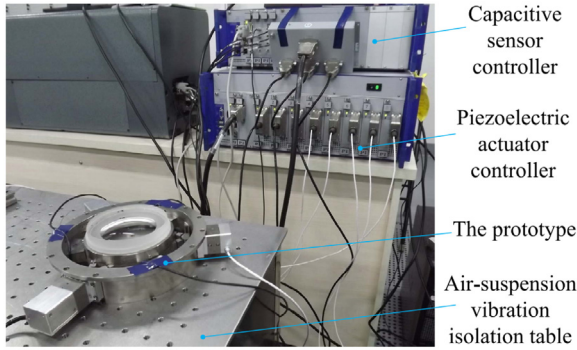

Fig. 12. Experimental system of the adjusting mechanism.

can be established. The measured transmission ratio result of the prototype is as below:

$$
\begin{bmatrix} D_1 \\ D_2 \\ D_3 \end{bmatrix} = \begin{bmatrix} 2.7548 & -0.4006 & -0.4705 \\ -0.4554 & 2.5690 & -0.4029 \\ -0.3879 & -0.4498 & 2.6093 \end{bmatrix} \begin{bmatrix} S_1 \\ S_2 \\ S_3 \end{bmatrix} \tag{9}
$$

Where, $\begin{bmatrix} D_1 & D_2 & D_3 \end{bmatrix}^T$ is the input displacement vector provided by the piezoelectric actuators, $\begin{bmatrix} S_1 & S_2 & S_3 \end{bmatrix}^T$ is the output displacement vector measured by the capacitive sensors. According to Eq. (9), when $S_1 = S_2 = S_3$, the transmission ratios corresponding to three group of kinematic chain are 1.8837, 1.7107 and 1.7716, respectively. According to Fig. 7, taken the average theoretical transmission ratio as 1.625, the error between the measured transmission ratios and the theoretical one are 15.92%, 5.27% and 9.02%. The error is mainly caused by two factors: Firstly, the flexible joints are taken as ideal hinges in theoretical calculation. The motion error of the flexible joints is not included for the simplification of calculation. Secondly, the manufacture error causes the transmission ratio error. To improve the calculation accuracy, the following aspects are worth trying. Firstly, the rotation precision of the flexible joints should be derived. The rotation center of the flexible joints is altered since the forces and moments acting on the flexible joints and produce elastic deformations [23]. This will change the value of l_b and b in Eq. (8) and directly affect the calculation result. Secondly, the equation of the proposed thinned fillet flexure hinge should be carefully derived since the accuracy of the adopted equation for the flexible joints will lead to the calculation error [24]. Finally, stiffness matrix method could be adopted instead of space vector method
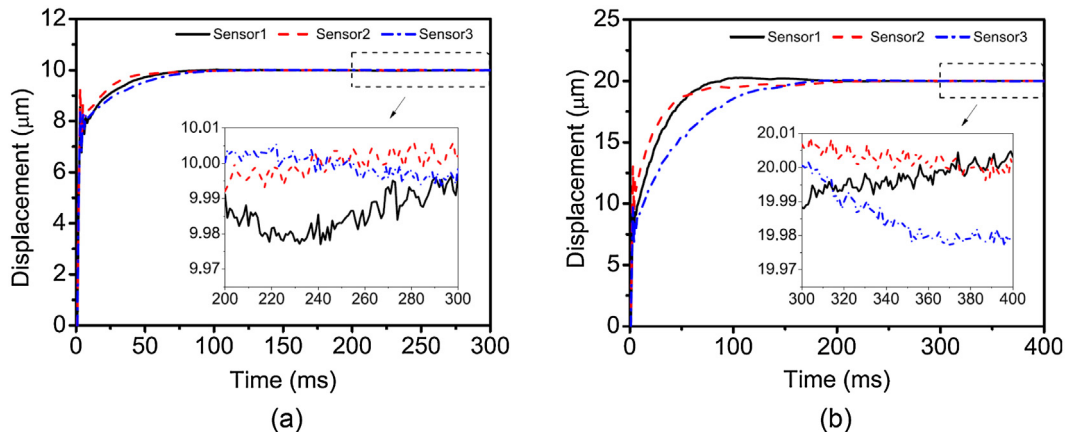

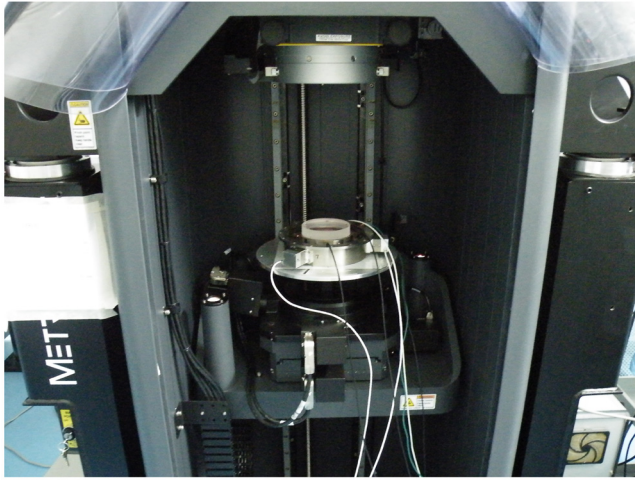Fig. 13. Displacement response curve of the capacitive sensors under different adjusting stroke: (a) 10 μm, (b) 20 μm.

Fig. 14. Surface figure measurement of the optical element for the adjusting mechanism.

Fig. 15. Surface figure of the optical element at different stroke.

results indicate that the adjusting force has little effect on the surface figure of the optical element.

5. Conclusions

In this research, a monolithic adjusting mechanism for optical element was proposed and developed, with the goal of achieving micrometer size adjusting stroke and nanometer size adjusting accuracy in a limited axial structure space for the application in the lithography objective lens. This mechanism is based on modified 6-PSS parallel mechanism with ordinary 6 pieces of prismatic joint reduced into 3. The thinned fillet flexure hinge is proposed to work as spherical joint for the realization of monolithic configuration.

The positional relationship between the input components and the output components of the adjustment mechanism is analyzed based on space vector method. Following from that, the transmission ratio expression is derived, which can be applied to determine the primary structural dimension of the adjustment mechanism. The parameters of flexible joints are determined by finite element analysis. The experimental results show that the adjusting stroke of the adjustment mechanism is 74.4 μm, adjusting accuracy is less than 40 nm and the surface figure variation of the optical element during the adjusting process is less than 1.5%.

All of the data verifies the feasibility of the flexible parallel mechanism to be applied as a monolithic adjusting mechanism in the lithography objective lens. The monolithic adjusting mechanism is also suitable for actuating other objects in the applications of micronano due to its compact structure, high adjusting accuracy and limited effect on actuated object. Further investigation will focus on the theoretical derivation of the stiffness and stress of the adjustment mechanism containing the effect of the flexible joints, and the optimization of the geometric parameters of the adjustment mechanism.

Acknowledgement

References

[1] B. Hoefflinger, Chips 2020: A Guide to the Future of Nanoelectronics, Springer-Verlag, Berlin, Heidelberg, 2012.
[2] T. Matsuyama, Y. Ohmura, D.M. Williamson, The lithographic lens: its history and evolution, Proc. SPIE 6154 (2006) 615403, http://dx.doi.org/10.1117/12. 656163.
[3] X.L. Liu, Y.Q. Li, K. Liu, Polarization aberration control for hyper-NA lithographic projection optics at design stage, Proc. SPIE 9618 (2015) 96180H, http://dx.doi.org/10.1117/12.2193245.

to investigate the calculation interpretation of the whole adjusting mechanism, in which the effect of the flexible joints is involved [25]. The output stiffness and the input stiffness of the whole adjusting mechanism should be derived. Then, the transmission ratio of the adjusting mechanism is the ratio of the output stiffness and the input stiffness. In spite of the error, it is verified that the simplified theoretical calculation of the transmission ratio can be adopted for the preliminary evaluation of the adjusting mechanism.

4.4. Effect of adjusting force on surface figure of optical element

When the piezoelectric actuators provide input displacement and force to the adjusting mechanism, it will not only change the position of the optical element, but also acts on the optical element and causes its surface figure variation. In the lithographic objective lens optical system, if the axial position change of the optical element couples with the surface figure variation of the optical element, the aberration compensation solution of the optical system will be complicated, and the difficulty and uncertainty of aberration compensation will be increased. Therefore, the effect of the adjusting force acted on the surface figure variation of the optical element should be restricted as small as possible. The surface figure variation of the optical element during the adjusting process is measured by a laser interferometer (model Verifire Asphere, from Zygo, Inc.), as shown in Fig. 14. The laser interferometer is located at an environment well controlled room with the temperature fluctuation within 0.05 °C and vibration isolation level better than VC-D. Therefore, the surface figure measurement is slightly influenced by the surrounding. The nominal heat produce of each piezoelectric actuator is 100 mW. When the adjusting mechanism works, the temperature rise near the optical element is within 0.03 °C. It indicates that there will be very little deformation of the adjusting mechanism during the surface figure measurement. Therefore, the surface figure variation of the optical element is mainly caused by the adjusting force of the adjusting mechanism in the measuring process.

The measurement result at the typical stroke of 0 μm, 30 μm and 60 μm is shown in Fig. 15. Ten times measurement is implemented at each adjusting position. The piston and tilt of the optical element which reflect the rigid motion are eliminated in the surface figure evaluation. The surface figure average root-mean-square (RMS) values at the stroke of 0 μm, 30 μm and 60 μm are 2.832 nm, 2.858 nm and 2.864 nm, respectively. The variation amplitude of the surface figure RMS value at each stroke is less than 1.5%. These
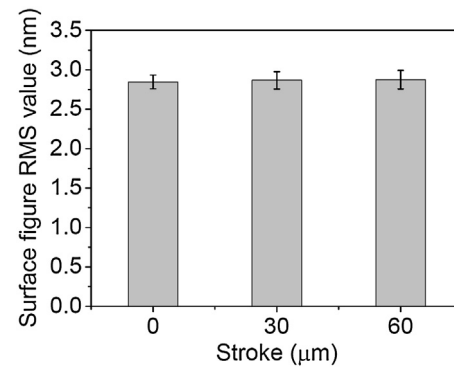
[4] H.W. Zhu, T.W. Xing, Z.X. Chen, Dynamic compensation for the lithographic object lens, Proc. SPIE 9195 (2014) 91950P, http://dx.doi.org/10.1117/12.2060302.

[5] Q.F. Guo, G. Jin, J.H. Dong, Y.C. Li, W. Li, H.P. Wang, Design and test of focusing mechanism of space camera, Proc. SPIE 7657 (2010) 76570X, http://dx.doi.org/10.1117/12.866449.

[6] Y.Q. Su, J.X. Zhang, T.Y. Lv, F. Yang, F.G. Wang, Mechanism design of continuous infrared lens, Proc. SPIE 8907 (2013) 890735, http://dx.doi.org/10.1117/12.2033240.

[7] H. Tajbakhsh, L. Hale, T. Malsbury, S. Jensen, J. Parker, Three-degree-of-freedom optic mount for extreme ultraviolet lithography, Proc. ASPE 18 (1998) 359–362.

[8] A.S. Gaunekar, G.P. Widdowson, N. Srikanth, G.N. Wang, Design and development of a high precision lens focusing mechanism using flexure bearings, Precis. Eng. 29 (2005) 81–85, http://dx.doi.org/10.1016/j.precisioneng.2004.05.005.

[9] T. Noll, K. Holldack, G. Reichardt, O. Schwarzkopf, T. Zeschke, Parallel kinematics for nanoscale Cartesian motions, Precis. Eng. 33 (2009) 291–304, http://dx.doi.org/10.1016/j.precisioneng.2008.07.001.

[10] D.J. Kluk, M.T. Boulet, D.L. Trumper, A high-bandwidth, high-precision, two-axis steering mirror with moving iron actuator, Mechatronics 22 (2012) 257–270, http://dx.doi.org/10.1016/j.mechatronics.2012.01.008.

[11] Y.F. Lu, D.P. Fan, Z.Y. Zhang, Theoretical and experimental determination of bandwidth for a two-axis fast steering mirror, Optik 124 (2013) 2443–2449, http://dx.doi.org/10.1016/j.ijleo.2012.08.023.

[12] Z.J. Jing, M.L. Xu, B. Feng, Modeling and optimization of a novel two-axis mirror-scanning mechanism driven by piezoelectric actuators, Smart Mater. Struct. 24 (2015) 025002, http://dx.doi.org/10.1088/0964-1726/24/2/025002.

[13] T.Y. Zhou, Y. Chen, C.Y. Lu, D.Y. Fu, X.P. Hu, Y. Li, B. Tian, Integrated lens auto-focus system driven by a nut-type ultrosonic motor (USM), Sci. China Ser. E: Technol. Sci. 52 (2009) 2591–2596, http://dx.doi.org/10.1007/s11431-009-0246-6.

[14] T. Martin, U. Gengenbach, H. Guth, P. Ruther, O. Paul, G. Bretthauer, Silicon linkage with novel compliant mechanism for piezoelectric actuation of an intraocular implant, Sensor Actuat. A: Phys. 188 (2012) 335–341, http://dx.doi.org/10.1016/j.sna.2012.02.016.

[15] S.C. Chen, M.L. Culpepper, S. Jordan, Six-axis compliant mechanisms for manipulation of micro-scale fiber optics components, Proc. SPIE 6466 (2007) 64660P, http://dx.doi.org/10.1117/12.702140.

[16] E.F. Fitcher, A. Stewart-Platform based manipulator: general theory and practical construction, Int. J. Rob. Res. 5 (1986) 157–182, http://dx.doi.org/10.1177/027836498600500216.

[17] Z. Huang, L.F. Kong, Y.F. Fang, Mechanism Theory and Control of the Parallel Robot Manipulator, China machine press, Beijing, 1997 (In Chinese).

[18] T. Huang, B. Jiang, Determination of the carriage stroke of 6-PSS parallel manipulators having the specific orientation capability in a prescribed workspace, in: Proc IEEE International Conference on Robots & Automation, San Francisco, 2000, pp. 2382–2385.

[19] W. Dong, L.N. Sun, Z.J. Du, Design of a precision compliant parallel positioner driven by dual piezoelectric actuators, Sensor Actuat. A: Phys. 135 (2007) 250–256, http://dx.doi.org/10.1016/j.sna.2006.07.011.

[20] Z.J. Du, R.C. Shi, W. Dong, Kinematics modeling of a 6-PSS parallel mechanism with wide-range flexure hinges, J. Cent. South Univ. 19 (2012) 2482–2487, http://dx.doi.org/10.1007/s11771-012-1300-2.

[21] H.L. Shi, H.J. Su, N. Dagalakis, J.A. Kramar, Kinematic modeling and calibration of a flexure based hexapod nanopositioner, Precis. Eng. 37 (2013) 117–128, http://dx.doi.org/10.1016/j.precisioneng.2012.07.006.

[22] Z. Huang, J.F. Liu, Y.W. Li, 150-year unified mobility formula issue, J. Yanshan Univ. 35 (1) (2011) 1–14, http://dx.doi.org/10.3969/j.issn.1007-791X.2011.01.001, In Chinese.

[23] N. Lobontiu, Compliance Mechanisms: Design of Flexure Hinges, CRC Press, London, 2003.

[24] Y.K. Yong, T.F. Lu, D.C. Handley, Review of circular flexure hinge design equations and derivation of empirical formulations, Precis. Eng. 32 (2008) 63–70, http://dx.doi.org/10.1016/j.precisioneng.2007.05.002.

[25] Y.M. Li, Q.S. Xu, Design and analysis of a totally decoupled flexure based XY parallel micromanipulator, IEEE Trans. Rob. 25 (2009) 645–657, http://dx.doi.org/10.1109/TRO.2009.2014130.

Biographies

Kang Guo received his BEng degree and the PhD degree in mechanical engineering from Jilin University, China in 2006 and 2011, respectively. He joined Changchun Institute of Optics, Fine Mechanics and Physics (CIOMP), Chinese Academy of Science in 2011 after obtaining PhD. He is currently an associate professor in the State Key Laboratory of Applied Optics, CIOMP, China. His research interests are ultra-precise actuation and measurement technologies for optical-mechanical system.

Mingyang Ni received his BEng degree and MEng degree in mechanical engineering from Jilin University, China in 2007 and 2009, respectively. He joined CIOMP in 2009 after obtaining MEng. He is currently an assistant professor in the State Key Laboratory of Applied Optics, CIOMP, China. His research interests are design and alignment technologies for precise optical-mechanical structure.

Huanan Chen received his BEng degree in mechanical engineering from Harbin Engineering University, China in 2007, and MEng degree in mechanical engineering from Harbin Institute of technology, China in 2011. Now, he is an assistant professor in the State Key Laboratory of Applied Optics, CIOMP, China. His research interests are design technologies for precise optical-mechanical structure.

Yongxin Sui received his BEng degree and MEng degree in optical engineering from Changchun University of Science and Technology, China in 1993 and 1996, respectively. He earned a PhD degree in optical engineering from CIOMP, Chinese Academy of Science in 2002. Now, he is a professor and heads the Engineering Research Center of Extreme Precision Optics of State Key Laboratory of Applied Optics, CIOMP, China. His research interests are extreme precision optical testing technology and optical information fusion technology.